

*Original Article*

# Comparative activities of Titania, Ni-Titania and Co-Titania in photocatalytic degradation of picric acid dye

Ezekiel Oluyemi Odebunmi<sup>1</sup> and Omolola Titilayo Odeyemi<sup>2\*</sup><sup>1</sup> *Department of Chemistry, Faculty of Physical Sciences,  
University of Ilorin, Ilorin, Nigeria*<sup>2</sup> *Department of Science Laboratory Technology, Institute of Applied Sciences,  
Kwara State Polytechnic, Ilorin, Nigeria*

Received: 23 January 2019; Revised: 27 July 2019; Accepted: 4 August 2019

---

**Abstract**

Titania (TiO<sub>2</sub>) photocatalyst was synthesized by the sol-gel method involving acid hydrolysis followed by oxidation with hydrogen peroxide. Cobalt and nickel metal ions were impregnated at 1, 5 or 10 % concentrations using metal nitrate salt solutions. The photocatalysts were characterized by various techniques. Scanning Electron Microscopy (SEM) and Diffused Reflectance Spectroscopy (DRS) showed that the doped TiO<sub>2</sub> were smaller in size and had smaller band gap than pure TiO<sub>2</sub>, while X-ray Diffraction (XRD) and X-ray Fluorescence (XRF) spectroscopy showed that all the photocatalysts were rutile phase and contained the expected elements. The percent degradation of Picric acid dye at pH 3, initial dye concentration 10 ppm, catalyst concentration 0.10 g/l, and temperature 55 °C, had rank order: TiO<sub>2</sub> < 1 % doped < 5 % doped < 10 % doped TiO<sub>2</sub>, showing that the photocatalytic activities of the Co-TiO<sub>2</sub> and Ni-TiO<sub>2</sub> increased with dopant concentration.

**Keywords:** Titania, Cobalt-titania, Nickel-titania, picric acid dye, and photocatalysts

---

**1. Introduction**

Access to clean water has become a major world-wide concern. Meanwhile, everyday human activities such as dyeing and production of textiles, cosmetics, drugs and paper have polluted several water bodies by discharges. Waste waters released when untreated or inadequately treated get into rivers, seas, lakes and groundwater, and these are then consumed by people, animals and plants without proper purification (Okereke, Ogidi, & Obasi, 2016). Picric acid (2,4,6-trinitrophenol) dye, for example, is a by-product from nitration of benzene, and this is done in the preparation of other dyes, fungicides and explosives (Goel & Singh, 2013).

Photocatalysis is an advanced oxidation process used to treat various dyes and pollutants (Kulkarni & Thakur, 2014). Photocatalysis is the excitation of a semiconductor

substance, such as titanium dioxide (TiO<sub>2</sub>), by photons (UV irradiation) to produce charge carriers: conduction band electrons (e<sup>-</sup>) and valence band holes (h<sup>+</sup>). The charge carriers induce reduction and oxidation reactions respectively, and degrade toxic compounds to less harmful products (Colmeares & Luque, 2013).

Recent studies have observed that a photocatalysts' activity can be improved by doping, meaning incorporating other elements or compounds into the structure of the photocatalyst (Mohd & Mahani, 2018; Odeyemi, Owalude, & Odebunmi, 2018; Razali, Mohd Noor, & Yusoff, 2017). Cobalt and Nickel metals possess 3d bands, which are between the conduction and valence bands of Titania, capable of providing sub-band gap. Then low energy photons can excite electrons from the valence band to dopant d-band, and from the dopant d-band to the conduction band. This process equally prevents premature recombination of charge carriers, which could stop the reaction (Ibhadon & Fitzpatrick, 2013).

This study investigated the activities of synthesized TiO<sub>2</sub> along with doped Co-TiO<sub>2</sub> and Ni-TiO<sub>2</sub> photocatalysts,

---

\*Corresponding author

Email address: lolaoyeus@yahoo.com

specifically in the degradation of picric acid dye.

## 2. Materials and Methods

### 2.1 Materials

Titanium trichloride (Tianjin Damao Chemicals, China), concentrated hydrochloric acid (BDH Laboratory Poole, England), 95% ethanol (BDH Laboratory Poole, England), ammonia solution and hydrogen peroxide (Sigma-Aldrich) were all used without further purification.

### 2.2 Synthesis of undoped and doped TiO<sub>2</sub>

Modifying the the sol-gel method by Molea & Popescu, 2011 and Wang, Liu, Wei, Dai, & Li, 2015; a 100 cm<sup>3</sup> sample of 10 % TiCl<sub>3</sub> containing 15 % HCl solution was refluxed with 100 cm<sup>3</sup> distilled water and 150 cm<sup>3</sup> 30 % NH<sub>3</sub> solution for 24 hours at 70 °C. After cooling the resulting solution, 50 cm<sup>3</sup> of 30 % H<sub>2</sub>O<sub>2</sub> was added. The yellow suspension that developed was aged for 12 hours and heated for 4 hours at 70 °C to produce a gel-like substance. The gel was dissolved in water, autoclaved at 100 °C for 24 hours, filtered and washed. The residue was oven-dried for 1 hour at 70 °C, ground, and calcined at 450 °C for 1 hour to obtain TiO<sub>2</sub> powder.

A 0.06 g (1 % w/w) sample of Ni (NO<sub>3</sub>)<sub>2</sub> salt was dissolved in 100 cm<sup>3</sup> distilled water and ethanol (3:1 v/v) (Kumar, Hitkari, Singh, Gautam, & Pandey, 2015). Then, 5.94 g (99 % w/w) TiO<sub>2</sub> was added and refluxed for 4 hours at 70 °C. After cooling, the resultant solution was filtered and the residue oven-dried at 70 °C for 1 hour, ground and calcined at 450 °C for 1 hour to obtain 1% Ni-TiO<sub>2</sub> (Muneaki, Tomoko, Naoto, Toyokazu, & Shinya, 2015). The same procedure was followed for other doped photocatalysts at their respective dopant levels.

### 2.3 Characterization methods

The photocatalysts were characterized using Scanning Electron Microscopy (SEM), X-ray Diffraction (XRD) Crystallography, X-ray Fluorescence (XRF) and Diffuse Reflectance Spectroscopy (DRS) methods. The SEM images were recorded on a Scanning Electron microscope (Aspex 3020) at 20 kV accelerating voltage. The samples were coated with gold using Balzer's sputtering device before imaging. XRD crystallography patterns were obtained with a powder X-ray diffractometer (Bruker D8 Advance) AXS Germany model, using Cu-K $\alpha$  radiation, over the 2 $\theta$  range from 10° to 100° at steps of 0.020°. The XRF spectra were recorded on 3600B Energy Dispersive X-ray Fluorescence Spectrophotometer. The band gaps were obtained on a solid-state LAMB DA™ 1050 UV/Vis/NIR Diffuse Reflectance spectrometer. Quartz substrate was dipped into the suspension of the sample, then dried and placed in the spectrophotometer with one side in the sample beam and the other in the reference beam. Spectra were obtained for the photocatalysts, and the band gaps were calculated from the equation (Vijayalakshmi & Rajendran, 2012):

$$(Ah\nu)^{1/2} = \alpha(h\nu - E_g) \quad (1)$$

In the equation, E<sub>g</sub> = band gap energy, h = Planck's constant,  $\nu$  = frequency (1/s), A = constant,  $\alpha$  = optical absorption coefficient. From a plot of (Ah $\nu$ )<sup>1/2</sup> versus h $\nu$ , a curve was obtained, and the band gap was calculated from the intersection of a straight line drawn as a tangent to the h $\nu$ -axis. The dye degradation was monitored using a N4S UV-Visible Spectrophotometer.

### 2.4. Photocatalytic degradation process

A 400-ppm stock solution of Picric acid dye was prepared and lower concentrations were obtained by dilution. The absorbances of dye solutions were measured at 0 min when no catalyst was present. The solutions were placed in a photo reactor irradiated with 20 W UV-lamp and aerated. About 2 cm<sup>3</sup> samples were taken at regular time intervals of 15 mins for a maximum period of 120 mins to the absorbance measurement at 355 nm, which is the wavelength of maximum absorbance ( $\lambda_{max}$ ) of Picric acid (Montazerozohori, Nasr-Esfahani, & Joohari, 2012). Dye concentration, pH, catalyst concentration and temperature were parameters considered in the degradation process. The activity of each photocatalyst on the dye was measured in percent degradation according to the equation (Odeyemi *et al.*, 2018):

$$\% \text{ degradation} = \frac{A_0 - A}{A_0} \times 100. \quad (2)$$

A<sub>0</sub> and A are initial (at 0 min) and final absorbances, respectively.

The reaction parameters were varied to obtain the optimum for the degradation of the dye. From the absorbance values, a plot of natural logarithm (ln) of absorbance against time, t, was made motivated by the first-order rate equation:

$$\ln[A] = \ln[A_0] - kt \quad (3)$$

The slope of the plot then gives the first order rate constant, k, for the reaction. The case with the largest rate constant had the optimum conditions for dye degradation.

#### 2.4.1 Measurement of the effect of pH

Buffer solutions at pH 2-11 were prepared with an initial dye concentration of 5 ppm Picric acid. Initial absorbance was measured and 0.1 g/l of photocatalyst was added. At 30 °C, the solution in a 200 cm<sup>3</sup> glass flask was transferred to the reactor. Supernatant solution samples were taken at 15 min intervals up to 120 mins, and their absorbances were measured (Abo-Farha, 2010).

#### 2.4.2 Measurement of the effect of dye concentration

Several concentrations (5-30 ppm) of picric acid were prepared from the stock solution with buffer corresponding to the optimum pH. At 30 °C and 0.1 g/l catalyst, the degradation was carried out (Montazerozohori *et al.*, 2012).

### 2.4.3 Measurement of the effect of catalyst concentration

At the optimum pH and dye concentration, catalyst concentrations were varied between 0.1 - 0.35 g/l for the degradation reaction at 30 °C (Susheela, 2012).

### 2.4.4 Measurement of the effect of temperature

Temperature was varied within 30-60 °C for the degradation at otherwise optimal reaction conditions (Soares, Lansarin, & Moro, 2007).

### 2.5 Determination of activation energies of the photocatalysts

Motivated by the linear form of Arrhenius equation

$$\ln k = \ln A - \frac{E_a}{RT} \quad (4)$$

the  $\ln$  of rate constant was plotted against the reciprocal of temperature in Kelvin (Choquette-Labbe, Shewa, Lalman, & Shanmugam, 2014). Here  $A$  is a pre-exponential factor,  $E_a$  is the activation energy and  $R$  is the gas constant. The activation energies  $E_a$  for the uncatalyzed and catalyzed degradation reactions were determined from the slopes of the linear plots, and were compared to confirm catalysis (Odebunmi, 2013).

## 3. Results and Discussion

### 3.1 SEM

The SEM micrographs of the photocatalysts are presented in Figures 1 (a) – (g). The undoped TiO<sub>2</sub> particles are larger than the doped particles at close working distances (WD) of 22.21, 21.53, 21.37 and 21.24 mm for undoped TiO<sub>2</sub>, 1 % Co-TiO<sub>2</sub>, 5 % Co-TiO<sub>2</sub>, 10 % Co-TiO<sub>2</sub>, and 21.57, 21.43 and 21.24 mm for 1 % Ni-TiO<sub>2</sub>, 5 % Ni-TiO<sub>2</sub> and 10 % Ni-TiO<sub>2</sub> respectively. This is because the metal ions impregnated into the TiO<sub>2</sub> broke down larger particles into smaller sizes (Kumar *et al.*, 2015).

### 3.2 XRF

Elemental compositions of the photocatalysts were assessed from X-ray fluorescence spectra in Figures 2 (a) – (g) as summarized in Table 1. Neuwirthová, Matejka, Kutlakova, & Tomasek, (2012) used this technique to observe the elemental proportions in photocatalytic materials. In this work, only a single titanium peak was observed in the undoped TiO<sub>2</sub> spectrum, while other peaks attributed to the dopant ions were observed in the doped cases (Brouwer, 2010). The intensity of dopant ion peak increased proportionately as the concentration increased. Therefore, the undoped and doped TiO<sub>2</sub> contained the expected elements in the appropriate quantities.

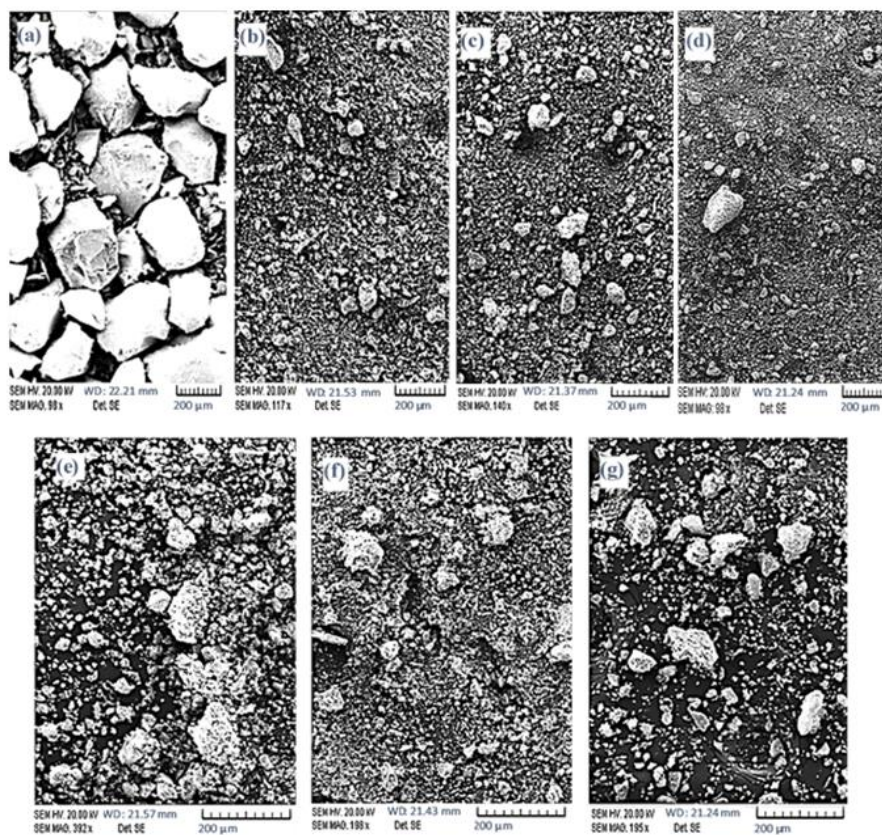


Figure 1. SEM micrographs of (a) TiO<sub>2</sub>, (b) 1 % Co-TiO<sub>2</sub>, (c) 5 % Co-TiO<sub>2</sub>, (d) 10 % Co-TiO<sub>2</sub>, (e) 1 % Ni-TiO<sub>2</sub>, (f) 5 % Ni-TiO<sub>2</sub>, and (g) 10 % Ni-TiO<sub>2</sub>.

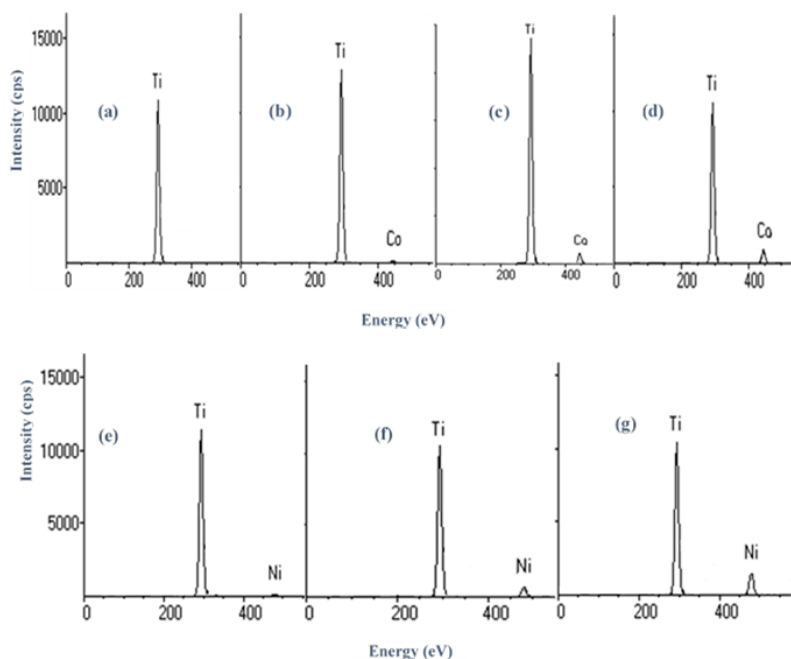


Figure 2. XRF spectra of (a) TiO<sub>2</sub>, (b) 1 % Co-TiO<sub>2</sub>, (c) 5 % Co-TiO<sub>2</sub>, (d) 10 % Co-TiO<sub>2</sub>, (e) 1% Ni-TiO<sub>2</sub>, (f) 5 % Ni-TiO<sub>2</sub>, and (g) 10 % Ni-TiO<sub>2</sub>.

Table 1. XRF data of the photocatalysts.

| Compositions of photocatalysts by weight % |                  |                         |                         |                          |                         |                         |                          |
|--------------------------------------------|------------------|-------------------------|-------------------------|--------------------------|-------------------------|-------------------------|--------------------------|
| Element                                    | TiO <sub>2</sub> | 1 % Co-TiO <sub>2</sub> | 5 % Co-TiO <sub>2</sub> | 10 % Co-TiO <sub>2</sub> | 1 % Ni-TiO <sub>2</sub> | 5 % Ni-TiO <sub>2</sub> | 10 % Ni-TiO <sub>2</sub> |
| Ti                                         | 96.19            | 96.93                   | 93.5                    | 93.04                    | 96.68                   | 95.19                   | 93.49                    |
| Co                                         | -                | 0.14                    | 1.42                    | 2.49                     | -                       | -                       | -                        |
| Ni                                         | -                | -                       | -                       | -                        | 0.24                    | 0.97                    | 2.25                     |
| Total                                      | 96.19            | 97.07                   | 94.92                   | 95.53                    | 96.92                   | 96.16                   | 95.74                    |

### 3.3 XRD

XRD spectra (Figures 3 a – g) show peaks corresponding to the rutile form of TiO<sub>2</sub> at 27.56 (110), 36.15 (101), 41.32 (111) and 54.30 (211) (Landmann, Rauls, & Schmidt, 2012). Insignificant peaks belonging to the brookite phase were also observed showing that the photocatalysts were a mixture of rutile and brookite phases. Dopant ion peaks were not observed in all the doped XRD patterns implying that crystal structures were not altered by the dopants (Mugundan *et al.*, 2015). All the peaks are in good agreement with the Joint Committee on Powder Diffraction (JCPD) data and similar to the standard spectrum for rutile TiO<sub>2</sub> (Landmann *et al.*, 2012). The photocatalysts have crystallite sizes of approximately 13, 12, 9, and 8 nm for TiO<sub>2</sub>, 1 % Co-TiO<sub>2</sub>, 5 % Co-TiO<sub>2</sub>, and 10 % Co-TiO<sub>2</sub>, and 12, 10 and 8.5 nm for 1 % Ni-TiO<sub>2</sub>, 5 % Ni-TiO<sub>2</sub>, and 10 % Ni-TiO<sub>2</sub> respectively according to the Debye-Scherrer formula (Bizarro & Rodil, 2015):

$$C_s = \frac{K\lambda}{\beta \cos\theta} \tag{5}$$

where C<sub>s</sub> = crystallite size, K = shape constant (0.89), λ = wavelength of measurement = 0.154184 nm, and β = full width at half maximum (FWHM) in radians.

### 3.4 DRS

The undoped titania has a direct band gap energy of 2.951 eV (Figure 4 a), which agrees with literature (Vijayalakshmi & Rajendran, 2012). The doped photocatalysts however, have reduced band gap energies of 2.636 and 2.793 eV for 10 % Co-TiO<sub>2</sub> and 10 % Ni-TiO<sub>2</sub> respectively (Figures 4 b – c). This reduction is attributed to the creation of a sub-band level between the valence band and the conduction band of rutile TiO<sub>2</sub> (Kumar *et al.*, 2015). The 10 % doped TiO<sub>2</sub> were selected as representative for the DRS analysis to observe effects from the maximum reduction in band gap.

### 3.5 Photocatalytic degradation of picric acid dye

From the typical first order plot (Figure 5) for the picric acid degradation, the rate constant for each reaction was obtained, and an R<sup>2</sup> value of 0.99 indicated a good linear least squares fit.

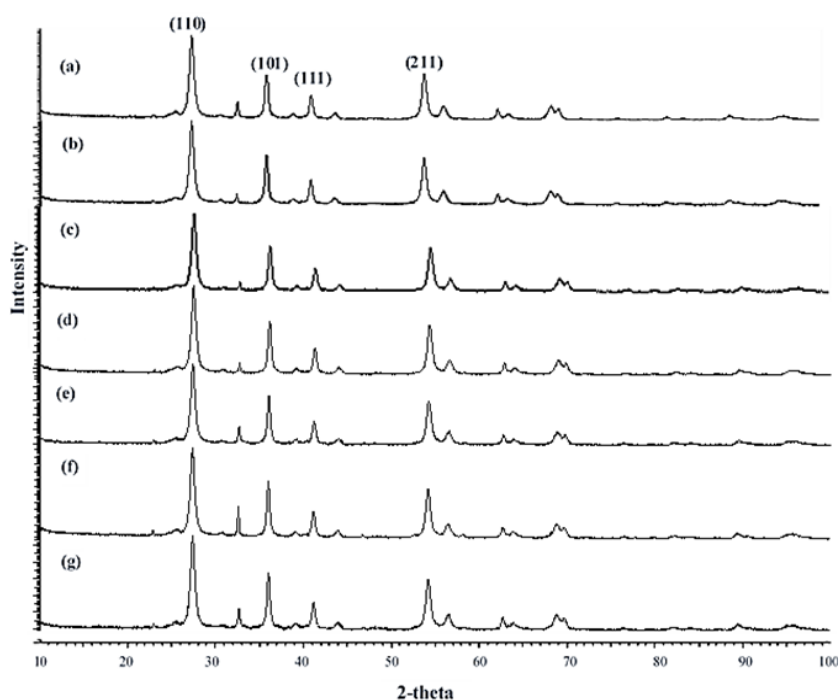


Figure 3. XRD spectra of (a) TiO<sub>2</sub>, (b) 1% Co-TiO<sub>2</sub>, (c) 5% Co-TiO<sub>2</sub>, (d) 10% Co-TiO<sub>2</sub>, (e) 1% Ni-TiO<sub>2</sub>, (f) 5% Ni-TiO<sub>2</sub>, and (g) 10% Ni-TiO<sub>2</sub>.

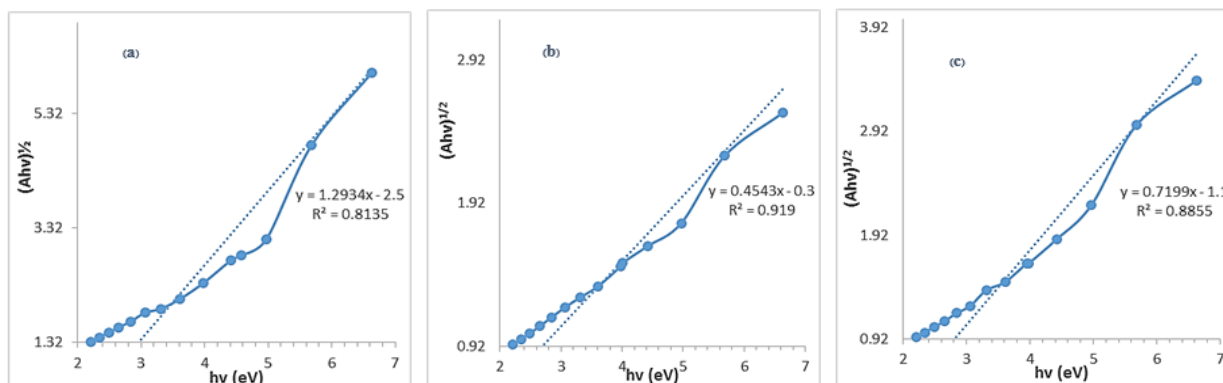


Figure 4. DRS band gaps of (a) TiO<sub>2</sub>, (b) Co-TiO<sub>2</sub>, and (c) Ni-TiO<sub>2</sub>.

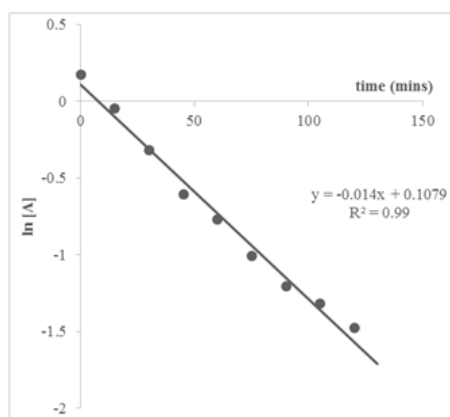


Figure 5. First order plot for Picric acid degradation at pH 3, initially 10 ppm dye, 0.1 g/l catalyst and 55 °C.

### 3.5.1 Effect of pH

Figure 6 (a) shows that, as the pH of the dye solution increased from 2 to 3, the rate constant for the degradation of picric acid dye increased. The dye was rapidly degraded at a highly acidic pH. The picric acid dye is negatively charged because of the electron withdrawing group, NO<sub>2</sub>, in its structure, while the surface of the catalyst is protonated by the hydrogen ion (H<sup>+</sup>) in solution at acidic pH (Guillard *et al.*, 2003; Konstantinou & Albanis, 2004). As a result, the positive charge induced on the catalyst and the negative charge on the dye attracted each other, facilitating degradation (Behnajady, Modirshahla, & Shokri, 2005). As the pH increased, H<sup>+</sup> concentration decreased while the negative ions increased making the catalyst surface completely negative. The negative charges on the catalyst and dye molecules then repelled each other. Photocatalytic degradation

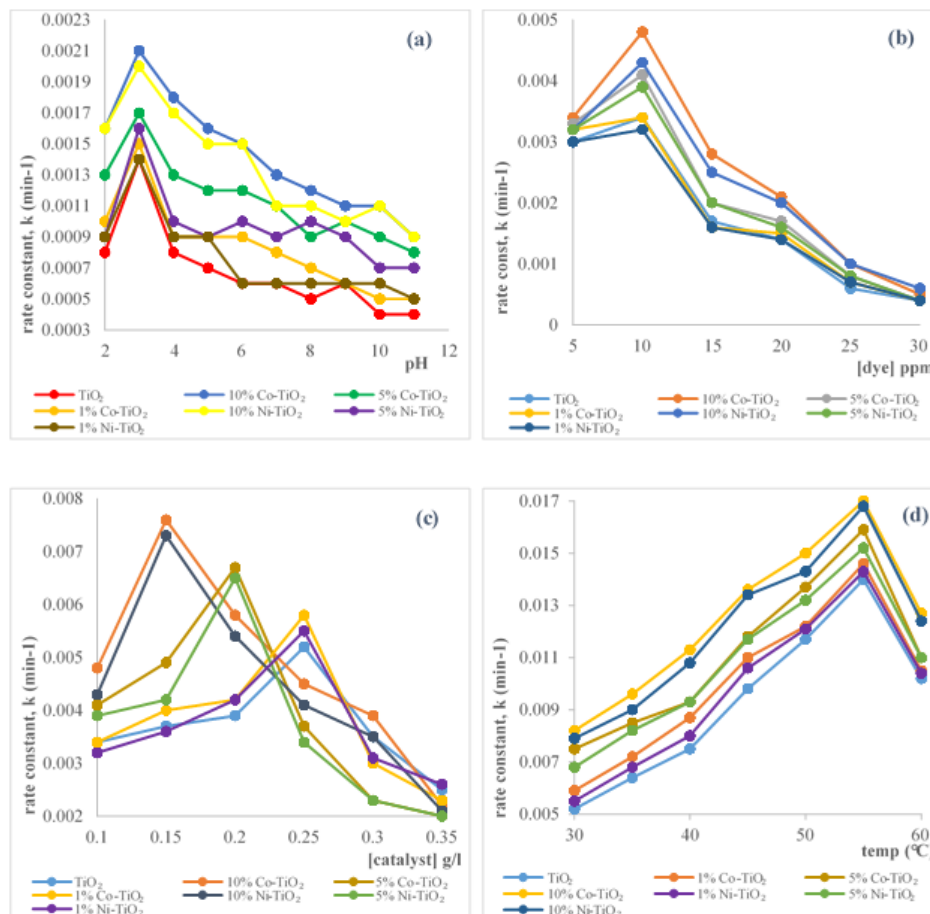


Figure 6. Variation of rate constant with (a) pH, (b) dye concentration, (c) catalyst concentration, and (d) temperature.

of the dye was enhanced by an acidic pH and inhibited by an alkaline pH for all the photocatalysts (Stephen, Micheal, & William, 2015).

### 3.5.2 Effect of dye concentration

Rate constant for the dye degradation in Figure 6 (b) increased first from 5 ppm reaching a maximum at 10 ppm, and then decreased from 15 to 30 ppm under otherwise similar degradation conditions. The initial increase resulted from more active sites on the catalyst than dye molecules in solution, while the subsequent decrease in rate constant resulted from more dye molecules than there were catalyst sites. Thus, the absorbance of the supernatant solution increased as dye concentration increased (Reza, Kurny, & Gulshan, 2017). The excess dye molecules blocked the UV-light from illuminating the catalyst surface hence reducing degradation rate (Saqib & Muneer, 2003). Although the optimum dye concentration obtained was 10 ppm for all the photocatalyst, more dye molecules were degraded by the doped catalysts.

### 3.5.3 Effect of catalyst concentration

The degradation rate of picric acid increased with catalyst concentrations from 0.1 g/l to 0.35 g/l (Figure 6 c) reaching a different optimum for each photocatalyst. At first,

more active sites were found on the catalyst, which were sufficient for the dye molecules, thus increasing the degradation rate (Saqib & Muneer, 2003). Beyond the optimum catalyst concentration, less dye molecules occupied the sites leaving empty sites on the catalysts surface, which increased the turbidity of the solution and prevented UV-irradiation from being absorbed by the catalyst (Gogate & Pandit, 2004; Li & Chen, 2011). Optimum catalyst concentrations found were 0.15, 0.20 and 0.25 g/l for the 10 %, 5 % and 1 % doped TiO<sub>2</sub> respectively and 0.25 g/l for the undoped TiO<sub>2</sub>. This was so because the area of active sites exposed to degradation increased as the dopants were introduced and equally increased as percent dopant concentration increased (Gogate & Pandit, 2004).

### 3.5.4 Effect of temperature

From Figure 6 (d), the degradation rate constant increased with temperatures from 30 °C up to a maximum of 55 °C, which is in good agreement with literature (Mozia, Morawski, Toyoda, & Inagaki, 2009). At low temperatures the adsorption of dye molecules and final product was favoured, while desorption of the products which tends to inhibit the reaction was not favoured. When the temperature was raised above the optimal 55 °C, degradation rate decreased. This was because adsorption of the dye, which is the rate limiting step,

becomes disfavored while desorption was enhanced. The doped TiO<sub>2</sub> cases were also found to have higher degradation rates at all the temperatures tested, than the undoped catalyst, because the energy levels introduced by the dopant ion into the band structure of the TiO<sub>2</sub> reduced the recombination of the charge carriers at the various temperatures (Mamba, Mamo, Mbianda, & Mishra, 2014).

### 3.6 The activation energies

Activation energies of the uncatalyzed and catalyzed dye degradation reactions (Table 2) were obtained from the slopes of the various Arrhenius plots (Figure 7). The activation energy of the uncatalyzed reaction was higher than of the catalyzed reactions, confirming true catalysis (Odebunmi, 2013; Odebunmi, Ogunlaja, & Owalude, 2010). Also, the activation energies decreased as the dopant concentration increased. This decrease indicates higher efficiency of the doped than undoped photocatalysts and much higher than of the uncatalyzed reaction. All the values obtained fall within the range of activation energies reported in prior literature for photocatalytic degradation reactions, which is 5-55 KJ mol<sup>-1</sup> (Shah *et al.*, 2003).

### 3.7 Comparison of photocatalytic activities

Maximum dye degradation with and without catalyst was 87 % and 4.6 %, respectively (Figures 8 a - b). This amounts to about 21 times more activity when catalyzed than when not catalyzed. Among the photocatalysts, the undoped TiO<sub>2</sub> gave the least degradation, which is attributed to a wider band gap than when doping the photocatalyst. The dye degradation also increased as dopant concentration increased, because the energy level created by the higher dopant concentration was closer to the valence band than with lesser dopant concentrations. As a result, more holes in the valence band were created in the former case. The cobalt and nickel dopants produced almost equal degradation rates at the equal doping levels of 1 %, 5 % or 10%.

## 4. Conclusions

In the synthesized Ni-TiO<sub>2</sub> and Co-TiO<sub>2</sub> catalysts, the metal ions increased the photocatalytic activity of TiO<sub>2</sub>. The characterization studies showed increasing activity of the photocatalysts in the rank order: undoped < 1 % doped < 5 % doped < 10 % doped TiO<sub>2</sub>. Degradation occurred both in the presence and absence of photocatalysts, but the catalysts increased both rate and extent of degradation.

## References

Abo-Farha, S. A. (2010). Photocatalytic degradation of monoazo and diazo dyes in wastewater on nanometer-sized TiO<sub>2</sub>. *Researcher*, 2(7), 1–20.

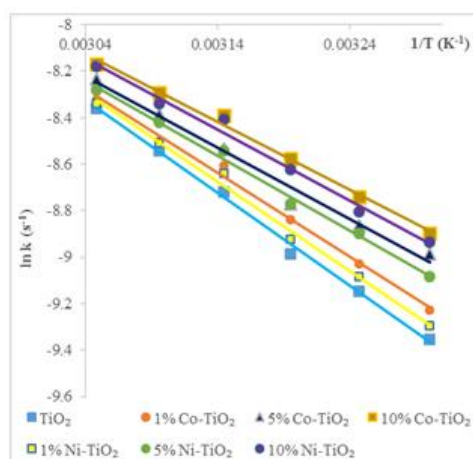


Figure 7. Arrhenius plot for Picric acid degradation.

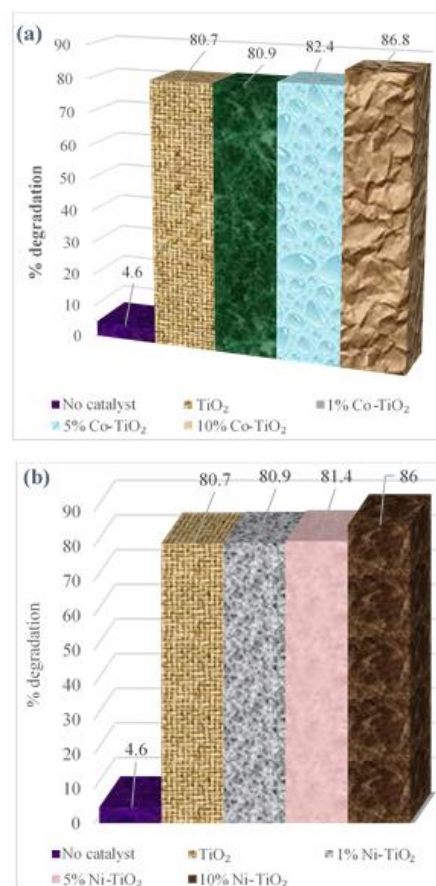


Figure 8. Comparison of activities of (a) TiO<sub>2</sub> and Co-TiO<sub>2</sub>, and (b) TiO<sub>2</sub> and Ni-TiO<sub>2</sub> photocatalysts with not catalyzed degradation reaction.

Table 2. Activation energies for not catalyzed and catalyzed Picric acid degradation.

| Activation energies of the photocatalysts                              |                  |                         |                         |                          |                         |                         |                          |               |  |
|------------------------------------------------------------------------|------------------|-------------------------|-------------------------|--------------------------|-------------------------|-------------------------|--------------------------|---------------|--|
| Photocatalyst                                                          | TiO <sub>2</sub> | 1 % Co-TiO <sub>2</sub> | 5 % Co-TiO <sub>2</sub> | 10 % Co-TiO <sub>2</sub> | 1 % Ni-TiO <sub>2</sub> | 5 % Ni-TiO <sub>2</sub> | 10 % Ni-TiO <sub>2</sub> | Not catalyzed |  |
| E <sub>a</sub> (kJ mol <sup>-1</sup> s <sup>-1</sup> K <sup>-1</sup> ) | 33.19            | 30.0                    | 25.6                    | 24.4                     | 32.1                    | 26.8                    | 25.4                     | 35.90         |  |

- Behnajady, M. A., Modirshahla, N., & Shokri, M. (2005). Photodestruction of acid orange 7 (AO 7) in aqueous solutions by UV/H<sub>2</sub>O<sub>2</sub>: Influence of operational parameters. *Chemosphere*, 55, 129–134.
- Bizarro, M., & Rodil, S. E. (2015). Physicochemical characterization of photocatalytic materials. In A. Hernandez-Ramirez, & I. Medina-Ramirez (Eds.), *Photocatalytic semiconductors* (pp. 103–153). Cham, Switzerland: Springer International.
- Brouwer, P. N. (2010). *Theory of XRF*. PANalytical B V Lelyweg, Almelo. Retrieved from www.panalytical.com
- Choquette-Labbe, M., Shewa, W. A., Lalman, J. A., & Shanmugam, S. R. (2014). Photocatalytic degradation of phenol and phenol derivatives using a Nano-TiO<sub>2</sub> catalyst: Integrating quantitative and qualitative factors using response surface methodology. *Water*, 6, 1785–1806.
- Colmenares, J. C., & Luque, R. (2013). Heterogeneous photocatalytic nanomaterials: Prospects and challenges in selective transformations of biomass-derived compounds. *Chemical Society Reviews*, 43, 765–778.
- Goel, N., & Singh, U. P. (2013). Syntheses, structural, computational, and thermal analysis of acid–base complexes of picric acid with N-Heterocyclic bases. *Journal of Physical Chemistry A*, 117(40), 10428–10437.
- Gogate, P. R., & Pandit, A. B. (2004). A Review of Imperative Technologies for Waste Water Treatment I: Oxidation Technologies at ambient conditions. *Advanced Environmental Resources*, 8, 501–551.
- Guillard, C., Lachheb, H., Houas, A., Ksibi, M., Elaloui, E., & Hermann, J. M. (2003). Influence of chemical structure of dyes, of pH and of inorganic salts on their photocatalytic degradation by TiO<sub>2</sub> comparison of the efficiency of powder and supported TiO<sub>2</sub>. *Journal of Photochemistry Photobiology A*, 158, 27–36.
- Ibhadon, A. O., & Fitzpatrick, P. (2013). Heterogeneous photocatalysis: Recent advances and applications. *Catalysts*, 3, 189–218.
- Konstantinou, I. K., & Albanis, T. A. (2004). TiO<sub>2</sub>-assisted photocatalytic degradation of azo dyes in aqueous solution: Kinetic and mechanistic investigations a review. *Applied Catalysis B: Environmental*, 49, 1–14.
- Kulkarni, M., & Thakur, P. (2014). Photocatalytic degradation and mineralization of reactive textile azo dye using semiconductor metal oxide nanoparticles. *International Journal of Engineering Research and General Science*, 2(2), 245–254.
- Kumar, A., Hitkari, G., Singh, S., Gautam, M., & Pandey, G. (2015). Synthesis of Ni-TiO<sub>2</sub> nanocomposites and photocatalytic degradation of oxalic acid in waste water. *International Journal of Innovative Research in Science, Engineering and Technology*, 4(12), 12722–12731.
- Landmann, M., Rauls, E., & Schmidt, W. G. (2012). The electronic structure and optical response of rutile, anatase and brookite TiO<sub>2</sub>. *Journal of Physics: Condensed Matter*, 24, 1–6.
- Li, Y., & Chen, W. (2011). Photocatalytic degradation of Rhodamine B using nanocrystalline TiO<sub>2</sub>-zeolite surface composite catalysts: Effects of photocatalytic condition on degradation efficiency. *Catalysis Science and Technology*, 1, 802–809.
- Mamba, G., Mamo, M. A., Mbianda, X. Y., & Mishra, A. K. (2014). Nd, N, S-TiO<sub>2</sub> decorated on reduced graphene oxide for a visible light active photocatalyst for dye degradation: Comparison to its MWCNT/Nd, N, S-TiO<sub>2</sub> analogue. *Industrial and Engineering Chemistry Research*, 53(37), 14329–14338.
- Mohd, H. R., & Mahani, Y. (2018). Highly efficient CuO loaded TiO<sub>2</sub> nanotube photocatalyst for CO<sub>2</sub> photoconversion. *Materials Letters*, 221, 168–171.
- Molea, A., & Popescu, V. (2011). The obtaining of titanium dioxide nanocrystalline powders. *Journal of Optoelectronics and Advanced Materials-Rapid Communications*, 5, 242–246.
- Montazerzohori, M., Nasr-Esfahani, M., & Joohari, S. (2012). Photocatalytic degradation of an organic dye in some aqueous buffer solutions using nano titanium dioxide: A kinetic study. *Environmental Protection Engineering*, 38(3), 45–55.
- Mozia, S., Morawski, A. W., Toyoda, M., & Inagaki, M. (2009). Application of anatase-phase TiO<sub>2</sub> for decomposition of azo dye in photocatalytic membrane reactor. *Desalination*, 241(1–3), 97–105.
- Mugundan, S., Rajamannan, B., Viruthagiri, G., Shanmugam, N., Gobi, R., & Praveen, P. (2015). Synthesis and characterization of undoped and cobalt-doped TiO<sub>2</sub> nanoparticles via sol-gel technique. *Applied Nano Science*, 5, 449–456.
- Muneaki, Y., Tomoko, Y., Naoto, Y., Toyokazu, N., & Shinya, Y. (2015). The loading effect of silver nanoparticles prepared by impregnation and solution plasma methods on the photocatalysis of Ga<sub>2</sub>O<sub>3</sub>. *Nuclear Instruments and Methods in Physics Research Section B: Beam Interactions with Materials and Atoms*, 359, 64–68.
- Neuwirthová, L., Matejka, V., Kutlakova, M. K., & Tomasek, V. (2012). X-ray fluorescence spectrometry Analysis of Clay/ZnO composites. *Nano*, (23), 1–6.
- Odebunmi, E. O. (2013). *Catalysis and chemical industry development: A fruitful wedlock. The one hundred and thirty-eighth (138<sup>th</sup>) Inagural Lecture, University of Ilorin, Nigeria.*
- Odebunmi, E. O., Ogunlaja, A. S., & Owalude, S. O. (2010). Kinetics of oxidation of D-Arabinose and D-Xylose by Vanadium (V) in the presence of Manganese (II) as homogenous catalyst. *Journal of Chilean Chemical Society*, 55, 293–297.
- Odeyemi, O. T., Owalude, S. O., & Odebunmi, E. O. (2018). Photocatalytic degradation of alizarin red dye in aqueous solution using Titania-Nickel and Titania-Cobalt Nanocomposites. *Ife Journal of Science*, 20(3), 705–710.
- Okereke, J. N., Ogidi, O. I., & Obasi, K. O. (2016). Environmental and health impact of industrial wastewater effluents in Nigeria – A Review. *International Journal of Advanced Research in Biological Sciences*, 3(6), 55–67.

- Razali, M. H., Mohd Noor, A. F., & Yusoff, M. (2017). Hydrothermal synthesis and characterization of  $\text{Cu}^{2+}/\text{F}^-$  co-doped Titanium dioxide ( $\text{TiO}_2$ ) nanotubes as photocatalyst for methyl orange degradation. *Science of Advanced Materials*, 9, 1–10.
- Reza, K. M., Kurny, A. S., & Gulshan, F. (2017). Parameters affecting the photocatalytic degradation of dyes using  $\text{TiO}_2$ : A review. *Applied Water Science*, 7, 1569–1578.
- Saquib, M., & Muneer, M. (2003).  $\text{TiO}_2$ -mediated photocatalytic degradation of a triphenylmethane dye (gentian violet), in aqueous suspensions. *Dyes Pigments*, 56, 37–49.
- Shah, S. I., Huang, C. P., Chen, J. G., Doren, D., & Barteau, M. (2003). Semiconductor metal oxide nanoparticles for visible light photocatalysis. *Proceedings of the NSF Nanoscale Science and Engineering Grantees Conference*. Arlington, VA.
- Soares, E. T., Lansarin, M. A., & Moro, C. C. (2007). A study of process variables for the photocatalytic degradation of rhodamine B. *Brazilian Journal of Chemical Engineering*, 24(1), 29–36.
- Stephen, A. T., Micheal, G., & William, J. C. (2015). Influence of pH on fluorescent dissolved organic matter photodegradation. *Water Research*, 85, 266–274.
- Susheela, B. G. (2012). Photocatalytic degradation study of methylene blue solutions and its application to dye industry effluent. *International Journal of Modern Engineering Research*, 2(3), 1204–1208.
- Vijayalakshmi, R., & Rajendran, V. (2012). Synthesis and characterization of nano- $\text{TiO}_2$  via different methods. *Archives of Applied Science Research*, 4(2), 1183–1190.
- Wang, Q., Liu, X., Wei, X., Dai, J., & Li, W. (2015). Ferromagnetic property of Co and Ni doped  $\text{TiO}_2$  nanoparticles. *Journal of Nanomaterials*, 1–5.